Renewable Energy 186 (2022) 35–50

Contents lists available at ScienceDirect

Renewable Energy

journal homepage: www.elsevier.com/locate/renene

Thermodynamic assessment of a small-scale solar chimney

Cristiana Brasil Maia [a, *], Janaína de Oliveira Castro Silva [a, b]

[a] Pontifícia Universidade Católica de Minas Gerais, Av. Dom José Gaspar, 500. Coração Eucarístico, Belo Horizonte, MG, CEP 30535-901, Brazil
[b] Centro Tecnológico de Educação Tecnológica de Minas Gerais, Av. Amazonas, 7675, Nova Gameleira, Belo Horizonte, MG, CEP 30510-000, Brazil

ARTICLE INFO

Article history:
Received 7 October 2021
Received in revised form
7 December 2021
Accepted 26 December 2021
Available online 1 January 2022

Keywords:
Solar chimney
Energy and exergy analysis
Analytical model
Experimental prototype

ABSTRACT

In recent decades, the world is facing significant global population growth, leading to an energy use intensification. Due to the depletion of global energy resources, renewable sources can be used to replace or enhance conventional sources. Solar energy is a non-polluting and inexhaustible energy source. The solar chimney uses solar energy to heat the air and generate an updraft airflow, which can be used for electricity generation or agricultural drying. Most models from the literature predict the steady-state airflow parameters using fixed values for ambient temperature and solar radiation, or unsteady analysis using experimental data. In this paper, a comprehensive assessment of the unsteady airflow inside a small-scale prototype is presented. A mathematical model is used to predict the mass flowrate and the temperatures of the airflow throughout a year, on an hourly basis, and the results showed a good agreement with experimental data obtained in a small prototype. The performance of the system was evaluated, with a maximum exergy efficiency of 11%. The low energy and exergy efficiencies were mainly attributed to the small dimensions of the prototype.

1. Introduction

Brazil has extensive regions with high levels of incident solar radiation and substantial land areas available for solar thermal applications. Also, it has a strong tradition on the use of renewable energy sources, accounting for 2.9% of total global renewable energy capacity investment in 2020, growing 23%, the seventh consecutive year of growth. In 2020, Brazil ranked third globally in terms of cumulative renewable energy capacity, with 150 GW [1]. Since 2012, the Brazilian government has been giving encouraging the development of several renewable energy sources [2], but 62% of the operational power capacity of Brazil is due to hydropower [1]. It is important, therefore, to develop other uses of solar energy. The solar chimney is a power plant that generates electricity from solar energy at a low temperature [3]. It consists of a translucid collector, a central tower, and one or more turbines [4]. The ground surface is heated by the incident solar radiation, and it heats the air under the solar collector. Buoyancy forces generate an airflow toward the chimney. The hot air updraft is used to drive a turbine and generate electricity.

The first solar chimney was constructed in Manzanares in 1982–1983, able to produce 50 kW. The plant, with a 195 m high tower and a solar collector of 250 m in diameter [5], produced electricity for seven years and proved the system successful [6]. Based on the reliability of the technology, the Manzanares plant was used as a reference for most of the simulation studies of solar chimneys developed so far [7]. Nevertheless, given the low efficiency of conversion of solar to electric energy, large structures are required to ensure competitive generation prices. Small-scale devices can be used to dry agricultural products or to provide natural ventilation [8]. Although most of the studies in literature concern large structures, a few studies are found on small-scale solar chimneys.

The feasibility of a small solar chimney to dry agricultural products was evaluated in Brazil [9]. Coffee beans, bananas, and tomatoes were dried inside a 12.3 m tall prototype, and the drying capacity was estimated in 440 kg of products or 320 kg of product per m^3/s of airflow, based on the yearly average mass flow rate and data from the literature [10]. The time required to dry the products depends on the product type and mass. The coffee beans, bananas, and tomatoes required, respectively, 76 h, 139 h, and 130 h to reach the final desired moisture content. The average efficiency of the device was estimated at 7%. In a subsequent work [8], the authors performed a CFD analysis to assess the effect of the geometric parameters on the airflow characteristics. In 2010, a 12 m high solar chimney was built at the University of Zanjan, Iran. The

* Corresponding author.
E-mail address: cristiana@pucminas.br (C.B. Maia).

https://doi.org/10.1016/j.renene.2021.12.128
0960-1481/

experimental analysis allowed the assessment of different temperatures and air velocities on the airflow parameters [11]. A similar study was developed for a 2 m high solar chimney built at the University of Tehran, Iran [12]. The same authors presented an analytical model to evaluate the influence of geometric parameters and materials on the airflow, validating the model with experimental data from a 3 m high solar chimney [13]. The performance of a solar chimney 3 m high and with a 3 m collector diameter was experimentally evaluated by Fadaei et al. [14] on the campus of the University of Tehran. The solar chimney performance was evaluated by measuring the solar radiation, PCM temperature, absorber surface temperature, and airflow velocity, for one day, with and without a PCM material. An experimental investigation of water condensate on the surfaces of the canopy and its influence on the solar chimney performance was carried out by Al-Kayeim et al. [15]. The experiments were performed in a prototype with 7 m of diameter and 6.5 m height, in Malaysia (latitude 4°N). A mathematical model of a 7 m high solar chimney was developed by Ref. [16]. The authors performed a comprehensive analysis, including a design calculation for the turbine, the prediction of pressure and heat losses, and the selection of materials for the collector, the absorber plate, the chimney, and for a thermal energy storage system. A CFD analysis of a solar chimney with a tower diameter of 0.6 m was performed by Ref. [17]. The tower height was varied between 3 and 8 m, and the effect of the absorber plate diameter and the collector plate angle on the performance of the system was also evaluated. The same authors evaluated the effect of divergence angle of the chimney, ambient temperature, solar irradiance, and turbine efficiency on the performance of a divergent solar chimney [18]. In a subsequent work, the same authors presented experimental results of a 6 m high solar chimney with an inbuilt thermal energy storage system [19].

There are a few studies considering energy and exergy analysis of solar chimneys, but most of them concern large structures. The exergy efficiency of a 1000 m high solar chimney was predicted based on a simplified analytical model [20]. An exergy analysis of a solar chimney for desalination and power production was developed by Ref. [21], considering a prototype with a diameter of 244 m. Aligholami et al. [22] employed exergy analysis to evaluate the effect of geometrical parameters on the turbine, for tower heights of 2, 3, and 4 m. The main objective was, therefore, to use the exergy analysis on turbine generation power. The mathematical model was validated by a comparison of the results of the mathematical model with the Manzanares plant. In previous works of the authors of the present paper, an energy and exergy analysis of the airflow inside a small-scale solar chimney was developed based on experimental results of a 12.3 m high solar chimney, with [23] and without [24] the drying of bananas.

Many works from the literature describe mathematical models to assess the airflow characteristics in solar chimneys. CFD models predict a detailed description of the airflow velocity and temperatures. A steady-state analysis of the airflow inside a sloped solar chimney power plant (SCPP) was proposed by Koonsrisuk [25] for a fixed value of solar irradiation. The influence of the collector roof height on the performance of a small-scale solar chimney was numerically assessed by Ayadi et al. [26,27] using a CFD analysis. The computational results were validated with experimental measurements performed on a 3 m height prototype built in the South East of Tunisia, North Africa. The results were obtained for a fixed value of incident solar radiation of 800 W/m^2 and fixed temperature values for the collector inlet and chimney outlet. The power generated by a 194 m SCPP in six cities of Saudi Arabia was predicted by Abdelmohimen and Algarni [28], using a steady-state analysis. Monthly average temperatures and solar irradiation were used as input data, using values from the last 22 years obtained by NASA. A steady-state analysis of the influence of the collector radius, incident solar radiation, and turbine pressure drop on the performance of a SCPP was developed by Rabehi et al. [29]. Fixed values for the collector inlet temperature, convective heat transfer, pressure drop, and incident solar radiation were used as boundary conditions. The numerical simulation results were compared with Manzanares experimental data from the literature. An analysis of a 195 m high SCPP was developed by Torabi et al. [30], assessing the effect on the system performance of the collector radius, the divergent angle of the chimney, and the incident solar radiation, ranging from 200 to 800 W/m^2. A sloped collector solar chimney was investigated by Weli et al. [31], using fixed values for the collector inlet, collector surface, and ground surface temperatures, on monthly basis. The solar irradiation was predicted on monthly basis. Attig-Bahar et al. [32] presented an analysis of the steady flow inside a 1 MW SCPP in Tunisia, using fixed solar irradiation and ambient temperature for July as reference. A CFD analysis of a 9 m high sloped SCPP was carried out by Fallah and Valipour [33], varying the incident solar radiation between 100 and 800 W/m^2. Krumar Mandal et al. [34] presented an experimental and numerical analysis of the airflow inside a small-scale prototype of a solar chimney, with a tower height of 6 m, on Kolaghat, India (latitude 22.4°). The numerical analysis was developed using CFD techniques, for steady-state conditions. It was adopted a prescribed heat flux at the ground surface of 600 W/m^2, and a convective heat transfer in the collector. Radiative heat transfer rates were disregarded.

Analytical models predict global airflow parameters, such as outlet temperature and power generated. A steady-state analytical model for large-scale commercial solar chimneys was developed by Koonsrisuk and Chitsomboon [35]. A mathematical model for a SCPP with an external heat source to ensure uninterrupted power generation was developed by Aurybi et al. [36], using steady-state conditions and fixed solar radiation of 1000 W/m^2. A thermodynamic model for the power generation by large-scale SCPP was carried out [37], using as input data a range of environmental conditions, varying both ambient temperature and solar irradiation. A mathematical model was developed to study the effect of geometry on the performance of a SCPP [38]. The steady-state analysis was developed for a constant value of solar irradiation.

Some studies are found for unsteady-state conditions. A thermodynamic analysis of a SCPP with soil heat storage was developed [39]. The analysis was presented for 24 h of simulation, for a known distribution of solar radiation. A transient analysis of the performance of solar chimneys was developed [40,41]. The results were obtained for large-scale prototypes, with ambient conditions (solar radiation and ambient temperature) obtained from the TRNSYS database.

Most previous research has presented a steady-state analysis to investigate the airflow inside a solar chimney, using fixed values for solar radiation and ambient temperature. A small number of studies present an unsteady analysis, using a known distribution of the ambient conditions. Also, it was not found a mathematical model to predict the performance of a solar chimney in Brazil.

The novelty of the present paper is the development of a thermodynamic model of the airflow inside a 2.5 m high solar chimney, based on results for a 1-h interval for a whole year. A mathematical model was developed for the weather conditions (ambient temperature and solar radiation), which was used as input to obtain the airflow parameters (mass flowrate, ground surface, and outlet airflow temperatures) and energy and exergy efficiency of the airflow. The numerical results were compared to experimental data measured on a prototype designed and built in Belo Horizonte, Brazil.

2. Mathematical model

Fig. 1 represents the schematic and physical diagram of the solar chimney. D_c and D_t represent the diameter of the collector and tower, respectively. h_c and H_t represent the height of the collector and tower, respectively. A prototype built in Belo Horizonte, Brazil (Latitude: 19°55′15″S, Longitude: 43°56′16″W) was selected as the reference for the model configuration, which consisted of a device with $D_c = 5.0$ m, $h_c = 0.1$ m, $D_t = 0.2$ m and $H_t = 2.5$ m.

The mathematical model consists of the determination of the outlet airflow temperature, the mass flowrate, and the energy and exergy efficiencies of the system. The airflow parameters depend on the ambient temperature and the incident solar radiation. The energy and exergy efficiencies depend on an energy balance that considers the convective and radiative heat transfer rates between the system and the environment.

The total solar radiation incident I on a surface is given by the sum of three components: the direct radiation I_b, the diffuse radiation I_d, and the reflected radiation by the ground and environment neighbors to the system. Using an isotropic sky model, the radiation absorbed by the ground is given by Ref. [42]:

$$S = I_b R_b (\tau\alpha)_b + I_d (\tau\alpha)_d \left(\frac{1+\cos\beta}{2}\right) + \rho_{ground} I (\tau\alpha)_g \left(\frac{1-\cos\beta}{2}\right) \quad (1)$$

$(\tau\alpha)$ is the transmittance-absorptance product, evaluated for the direct (subscript b), diffuse (subscript d), and ground reflected (subscript g) radiation components. β represents the angle between the collector and a horizontal surface and ρ_{ground} is the ground reflectance. The mathematical model was implemented to environmental conditions of the city of Belo Horizonte, Brazil. The incident solar radiation is determined on an hourly basis, based on the daily values for the incident solar radiation and the clearness index obtained on the typical meteorological year for Belo Horizonte [43], as suggested by Ref. [42]. The results are presented for a 1-h interval, for the 365 days of the year.

The hourly ambient temperature was predicted based on [44] and uses the maximum, minimum, sunrise, and sunset temperatures, obtained using available data from the Brazilian System of Data Collection [45].

An energy balance was developed for the heat transfer rates of the solar collector, shown in Fig. 2. The convective heat transfer rate between the solar collector and the airflow inside the system is $q''_{conv,3}$ and the radiative heat transfer rate between the solar collector and the ground is $q''_{rad,1}$. The collector loses heat to the environment by convection ($q''_{conv,2}$) and radiation ($q''_{rad,2}$).

The heat conducted to the deeper ground layers ($q''_{cond,0}$) is determined through a heat balance in the ground as the difference between the solar radiation absorbed by the ground (S, given in Eq. (1)) and the heat leaving the ground surface. In this case, the energy leaving the ground surface is the heat transferred to the ground by convection ($q''_{conv,1}$), to the collector by radiation ($q''_{rad,1}$) and to the external environment by radiation ($q''_{rad,3}$), as given by:

$$S - q''_{conv,1} - q''_{rad,1} - q''_{rad,3} = q''_{cond,0} \quad (2)$$

The radiative heat transfer between the ground surface and the solar collector can be assumed as the radiation between two infinite flat plates, as presented by Ref. [42]. The net radiation flux exchanged with the collector is given by:

$$q''_{rad,1} = \frac{\sigma\left(T_{ground}^4 - T_{coll}^4\right)}{\frac{1}{\varepsilon_{coll}} + \frac{1}{\varepsilon_{ground}} - 1} \quad (3)$$

where ε_{coll} and ε_{ground} represent the collector and ground emittance, respectively. T_{ground} and T_{coll} represent the ground surface and collector temperatures, respectively.

The convective heat flow rate between the collector and the external airflow is given by:

$$q''_{conv,2} = h_{coll,\,amb}(T_{coll} - T_{ai}) \quad (4)$$

where the convective heat transfer coefficient $h_{coll,\,amb}$ can be estimated by Refs. [46–48]:

$$h_{coll,\,amb} = \frac{0.2106 + 0.0026\, V_{amb}\left(\frac{\rho T_m}{\mu g \Delta T}\right)^{\frac{1}{3}}}{\left(\frac{\mu T_m}{g \Delta T C_p k^2 \rho^2}\right)^{\frac{1}{3}}} \quad (5)$$

T_m is the average between the collector surface temperature and the ambient temperature. ΔT is the temperature difference

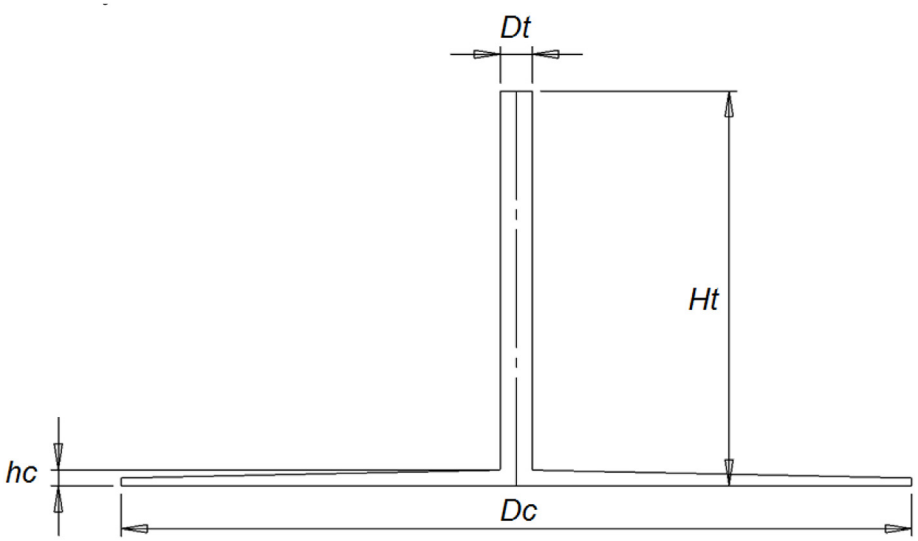

Fig. 1. Main geometric parameters.

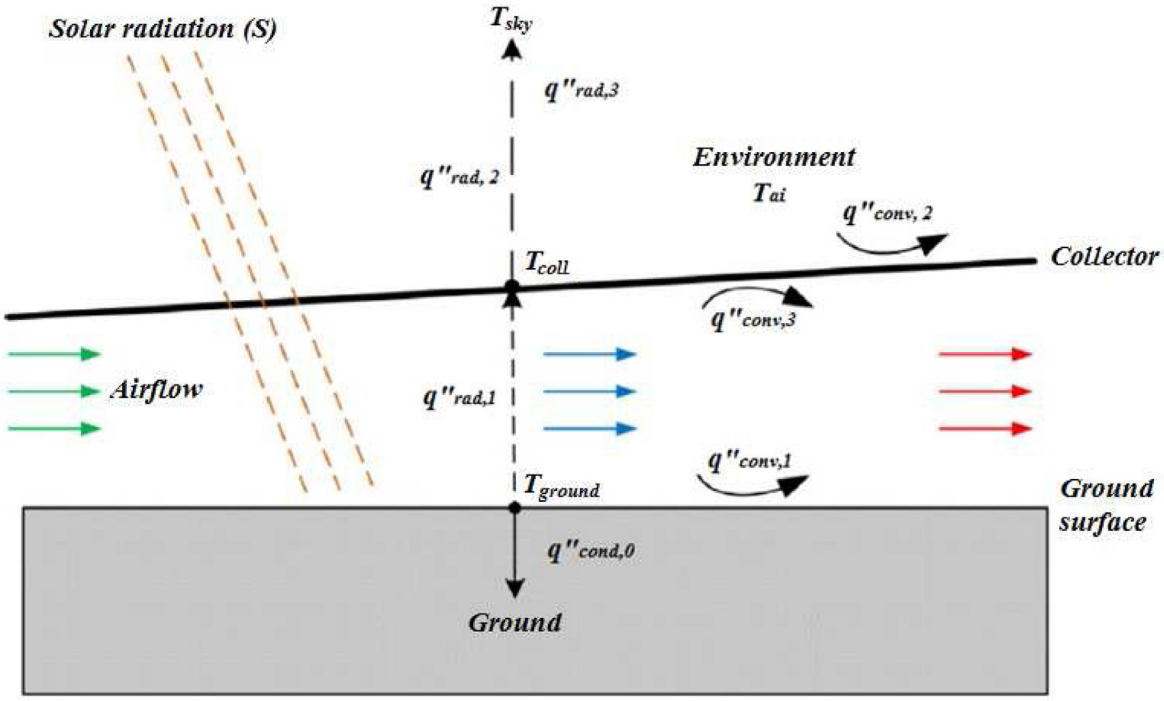

Fig. 2. Heat transfer rates.

between the airflow in the collector and the environment. ρ, μ, C_p and k stand for density, dynamic viscosity, specific heat at constant pressure, and thermal conductivity of air, respectively. V_{amb} is the wind velocity.

The radiative heat transfer rate between the collector surface and the sky can be assumed as the heat transfer by radiation from a small object enclosed by a large surface [42]:

$$q''_{rad,2} = \sigma \varepsilon_{coll}\left({T_{coll}}^4 - {T_{sky}}^4\right) \tag{6}$$

where T_{sky} is the effective sky temperature.

The convective heat transfer between the ground and the airflow inside the collector is given by:

$$q''_{conv,1} = h_{ground,\,esc}\left(T_{ground} - T_{ao}\right) \tag{7}$$

where T_{ao} is the average temperature of the air inside the collector. The convective heat transfer coefficient between the ground surface and the flow is given by Ref. [48]:

$$h_{ground,\,esc} = 3.87 + 0,0022\left(\frac{V\rho C_p}{Pr^{\frac{2}{3}}}\right) \tag{8}$$

where Pr is the Prandtl number of the air inside the collector. V is the average airflow velocity.

The radiative heat transfer rate between the ground and the environment can be estimated by,

$$q''_{rad,3} = \tau_{coll}\,\sigma \varepsilon_{ground}\left({T_{ground}}^4 - {T_{sky}}^4\right) \tag{9}$$

τ_{coll} is the infrared transmittance of the collector.

The temperature in a specific depth of the ground can be determined by the solution of the one-dimensional unsteady energy conservation equation. Assuming the ground as a semi-infinite solid [49], the temperature of the ground surface is given by Ref. [50]:

$$T_{ground}(t) = T_{ai} + \frac{2}{\sqrt{\pi}}\frac{\alpha'}{k_{ground}}\int_{t'=0}^{t}\frac{q''_{cond,0}(t')}{\sqrt{4\alpha'(t-t')}}dt' \tag{10}$$

α' is the thermal diffusivity of the ground.

The conductive heat transfer to the ground is given by

$$q''_{cond,0} = -k_{ground}\left.\frac{\partial T_{ground}}{\partial x}\right|_{x=0} \tag{11}$$

The convective heat transfer between the collector and the internal flow is given by:

$$q''_{conv,3} = h_{coll,\,esc}(T_{coll} - T_{ao}) \tag{12}$$

where the convective coefficient between the collector and the airflow $h_{coll,\,esc}$ is given by Refs. [46–48]:

$$h_{coll,\,esc} = \frac{\left(\frac{f}{8}\right)(Re_x - 1000)Pr}{1 + 12.7\left(\frac{f}{8}\right)^{\frac{1}{2}}\left(Pr^{\frac{2}{3}} - 1\right)}\left(\frac{k}{d_h}\right) \tag{13}$$

Re_x is the Reynolds number in the collector and d_h is the hydraulic diameter. Pr and k represent the Prandtl number and the thermal conductivity of air, respectively. The Darcy friction factor f is [51]:

$$f = (1.82\log_{10} Re_x - 1.64)^{-2}\ Re_x < 3.4\,x\,10^6 \tag{14}$$

The average temperature of the airflow at the system outlet is given by [12].

$$T_{ao} = \frac{q''_{conv,1}\pi}{\dot{m}\,C_p}\left[{R_c}^2 - \left(\frac{D_t}{2}\right)^2\right] + T_{ai} \tag{15}$$

The mass flowrate is determined by adapting the model of [52] for small solar chimneys [53].

$$\dot{m} = \sqrt[3]{\frac{\frac{\rho^2 \beta' g q''_{conv,1} \pi^3}{8 C p_{ao}} H_t \left[{R_c}^2 - \left(\frac{D_t}{2}\right)^2 \right]}{\frac{4 F_y H_t}{{D_t}^5} + \frac{\frac{F_x}{64}}{R_c {h_c}^3} + \frac{1}{{D_t}^4}}} \tag{16}$$

$\beta' \sqrt{a^2 + b^2}$ is the volumetric expansion coefficient. F_x represents the friction factor in the collector [51].

$$F_x = 0.046\, {Re_x}^{-\frac{1}{5}} \tag{17}$$

F_y represents the friction factor in the tower

$$\frac{1}{\sqrt{F_y}} = 1.5635 \ln\left(\frac{Re_x}{7}\right) \tag{18}$$

The energy efficiency of solar chimneys, neglecting the turbine efficiency, is given by [54].

$$\eta_{SP} = \left[\frac{\int \dot{m} C_p (T_{ao} - T_{ai}) dt}{A_{col} H_o}\right] \left[\frac{H_t g}{C_p T_{ai}}\right] \tag{19}$$

A_{col} represents the collector area, g is the gravity acceleration and H_o is the extraterrestrial radiation on a horizontal surface.

The exergy efficiency is defined by the ratio of total exergy output $\dot{E}x_{out}$ and input $\dot{E}x_{in}$ [23,24,55].

$$\varepsilon = \frac{\dot{E}x_{out}}{\dot{E}x_{in}} \tag{20}$$

The exergy input concerns the exergy flow rate due to the heat transfer and to the airflow entering the system, and the exergy output concerns the airflow leaving the system.

$$\dot{E}x_{in} = \left(1 - \frac{T_o}{T_{ground}}\right) \dot{Q} + \dot{m}_{ai} \psi_{ai} \tag{21}$$

$$\dot{E}x_{out} = \dot{m}_{ao} \psi_{ao} \tag{22}$$

$\dot{Q}$ is the heat transfer rate through the ground, given by the First Law of Thermodynamics, neglecting the energy utilization rate:

$$\dot{Q} = \dot{m}_{ao} \left[\left(h_{ao} + \frac{V_{ao}^2}{2}\right) - \left(h_{ai} + \frac{V_{ai}^2}{2}\right) \right] \tag{23}$$

T_o is the dead state temperature. ψ_{ai} and ψ_{ao} represent the outlet specific flow exergy. h_{ao} and h_{ai} represent the specific enthalpies of the airflow at the system outlet and inlet, respectively, and V_{ao} and V_{ai} represent the airflow velocities at the system outlet and inlet, respectively.

The inlet and outlet specific exergy flows are determined by Ref. [56]:

$$\begin{aligned}\psi_{ai} = {} & (C_{p,ai} + \omega_{ai} C_{p,v}) T_o \left(\frac{T_{ai}}{T_o} - 1 - \ln\frac{T_{ai}}{T_o}\right) \\ & + (1 + 1.6078\omega_{ai}) R_a T_o \ln\frac{P_{ai}}{P_o} + R_a T_o \Bigg[\\ & \times (1 + 1.6078\omega_{ai}) \ln\left(\frac{1 + 1.6078\omega_0}{1 + 1.6078\omega_{ai}}\right) + 1.6078\omega_{ai} \ln\left(\frac{\omega_{ai}}{\omega_0}\right) \\ & \times \Bigg] \sqrt{b^2 - 4ac}\end{aligned} \tag{24}$$

$$\begin{aligned}\psi_{ao} = {} & (C_{p,ao} + \omega_{ao} C_{p,v}) T_o \left(\frac{T_{ao}}{T_o} - 1 - \ln\frac{T_{ao}}{T_o}\right) \\ & + (1 + 1.6078\omega_{ao}) R_a T_o \ln\frac{P_{ao}}{P_o} + \\ & + R_a T_o \left[(1 + 1.6078\omega_{ao}) \ln\left(\frac{1 + 1.6078\omega_0}{1 + 1.6078\omega_{ao}}\right) \right. \\ & \left. + 1.6078\omega_{ao} \ln\left(\frac{\omega_{ao}}{\omega_0}\right) \right]\end{aligned} \tag{25}$$

where R_a is the air constant, P_o is the pressure in dead state, P_{ai} and P_{ao} are the air pressure in the inlet and outlet, respectively. $C_{p,v}$ is the specific heat of the water vapor, and ω_0 is the specific humidity of the flow in dead state.

3. Experimental setup

An experimental solar chimney system was installed and operated in Belo Horizonte, Brazil. Belo Horizonte has an Aw (Equatorial savannah with dry winter) climate [57,58]. The dimensions of the prototype were based on the device described by Refs. [9,24,59], on a 1:5 scale. The experimental results from the prototype were used to validate the mathematical model.

The tower was made with PVC tubes, to ensure a light and resistant structure. To avoid thermal losses for the environment, it was covered by an insulating material. The collector was made using a thermodiffuser film, normally used in greenhouses. The collector was kept elevated using vertical steel rods, with a diameter of 3/8". Since the diameter of the rods is small compared to the airflow cross-sectional area, it was assumed that the interference of the rods on the airflow is minimum.

The prototype was positioned on a blackened surface, to increase the energy absorbed and increase the air temperature. The absorptance of the ground surface was estimated at 97%. The ground surface was treated to avoid the migration of humidity from the ground to the airflow. Fig. 3 shows the system under construction, in which the blackened ground surface, the tower without thermal insulation, and the steel rods (before being cut) can be seen. Fig. 4 shows the experimental prototype when ready.

The ambient conditions were monitored using data from a meteorological station of GREEN PUC Minas, the research laboratory in which the system was installed. The evaluated parameters are total and diffuse components of solar radiation, wind speed, precipitation, humidity, and ambient temperature, using a Campbell datalogger, CR1000 model, a Kipp & Zonen pyranometer CM 6 B model, an Eppley pyrheliometer Nip model, and a Vaisala thermohygrometer, HMP45AC model. Solar radiation and ambient temperature were measured outside the prototype. The outlet airflow temperature was measured with a K-type thermocouple positioned at the center of the system outlet, with an accuracy of 0.58 °C. The relative humidity was measured with two thermohygrometers model HTR-157 (Instrutherm), with an accuracy of 0.1%. The first was positioned at the system inlet and the other, at

Fig. 3. Experimental prototype under construction.

Fig. 4. Experimental prototype.

the system outlet, to ensure that the airflow was not absorbing humidity from the ground. A schematic layout of the sensors is shown in Fig. 5. An uncertainty analysis was carried out using the methodology recommended by Moffat [60].

4. Results and discussion

The mathematical model was used to predict the hourly incident solar radiation and ambient temperature for each day of the year, for the city of Belo Horizonte, Brazil. Based on these results, the outlet temperature, the hourly ground surface temperature, and the mass flowrate were predicted for a device with the same geometry as the experimental prototype. Then, a thermodynamic analysis was performed and the hourly exergy and energy efficiencies were determined. The results of the airflow parameters were compared to experimental data, and the results are shown for one day at the beginning of Spring. Monthly average values are shown for ambient and airflow parameters.

4.1. Model validation

To ensure the consistency of the model, the experimental results obtained in the built prototype are compared with the numerical predictions of the ambient and airflow parameters obtained from the developed model. The comparison of the numerical and experimental ambient temperature is shown in Fig. 6, with the incident solar radiation. Due to the high levels of solar radiation, ambient temperature is high, reaching 33.5 °C (experimental data). As expected, there is a discrepancy between numerical and experimental data, attributed to the variation of the ambient conditions from year to year. For this reason, the Typical Meteorological Year (TMY) hourly ambient temperature for the day of the test is also shown in Fig. 6. The general behavior obtained is similar to the experimental results and the values are close, leading to the conclusion that the model results can represent the expected ambient temperature.

The ground surface is heated by the incident solar radiation, and it heats the air under the solar collector, which creates buoyancy forces that generate the airflow. Therefore, the ground surface temperature is an important parameter of the airflow, and it is presented in Fig. 7. The minimum and maximum differences observed between numerical and experimental values were 0.4 and 8.3 °C, respectively, with an average value of 4.7 °C. Considering that the ground surface temperature depends on the predicted solar radiation and the ambient temperature, it can be assumed that the ground surface temperature can be predicted by the proposed model.

The heated air under the solar collector accelerates through the bottom of the tower, leaving the systems through the top of the tower. The average outlet airflow temperature is higher than the inlet temperature but lower than the ground surface temperature, as can be seen in Fig. 8. The outlet airflow temperature behavior is similar to the ground surface temperature. The model predicted lower values for the airflow temperature compared to experimental results, following the lower values predicted for the ground surface temperature (Fig. 7). The numerical results from the airflow temperature showed greater agreement to the experimental data when compared to the ones for the ground surface temperature, with minimum, maximum and average differences of, respectively, 0.3, 5.0, and 1.8 °C.

4.2. Ambient and airflow parameters

The ambient, ground surface and outlet temperatures obtained were compared with experimental data for a specific day in October (Figs. 6–8). The results for one year of simulation, on an hourly basis, are shown in Figs. 9–11. It is observed a significant variation of the temperatures during the day.

Fig. 9 presents the ambient temperature distribution throughout the year. The yearly average was 23.9 °C, with minimum and maximum values of, respectively, 13.0 °C and 35.1 °C. During one day, it was observed a maximum variation of 15.7 °C. Fig. 10 presents the outlet airflow temperature. The yearly average was 27.4 °C, with minimum and maximum values of, respectively, 15.0 °C and 46.7 °C. During one day, it was observed a maximum variation of 27.8 °C.

Fig. 11 presents the ground surface temperature distribution, with a yearly average of 30.8 °C, and minimum and maximum values of, respectively, 15.0 °C and 59.4 °C. The maximum variation observed in one day was 40.8 °C. It is worth mentioning that the temperatures were obtained considering also the night period.

The incident solar radiation is considered the fundamental element of the solar chimney because it supplies the energy required to drive the airflow. Only a portion of this energy is absorbed by the ground surface and heats the airflow. Fig. 12 shows the solar radiation absorbed by the ground surface (S) and the ambient temperature, on a monthly average, based on the hourly data obtained for a year. The absorbed solar radiation and the ambient temperature are lower during the months from March to August, which correspond to the autumn and winter months in the southern hemisphere.

To allow better visualization, Fig. 13 shows the solar radiation absorbed by the ground surface and the ambient temperature variation during a specific day in October. The maximum value observed was 647 W/m^2. It is worth mentioning that the absorbed solar radiation shown in Fig. 12 is lower than the peak of the

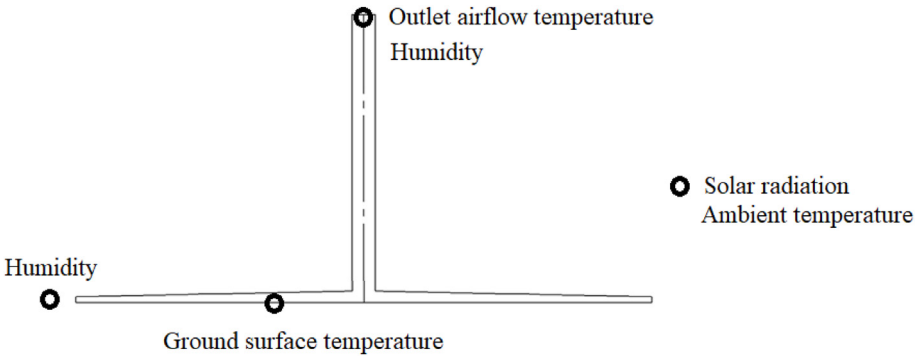

Fig. 5. Schematic layout of the sensors.

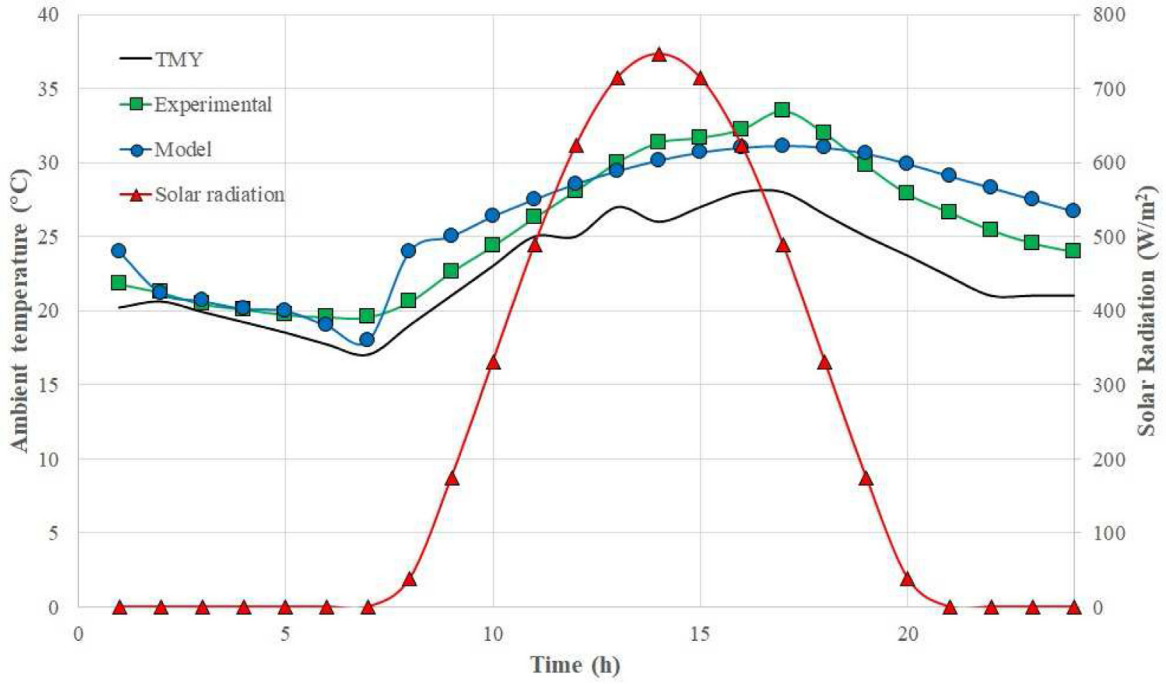

Fig. 6. Validation of the ambient temperature.

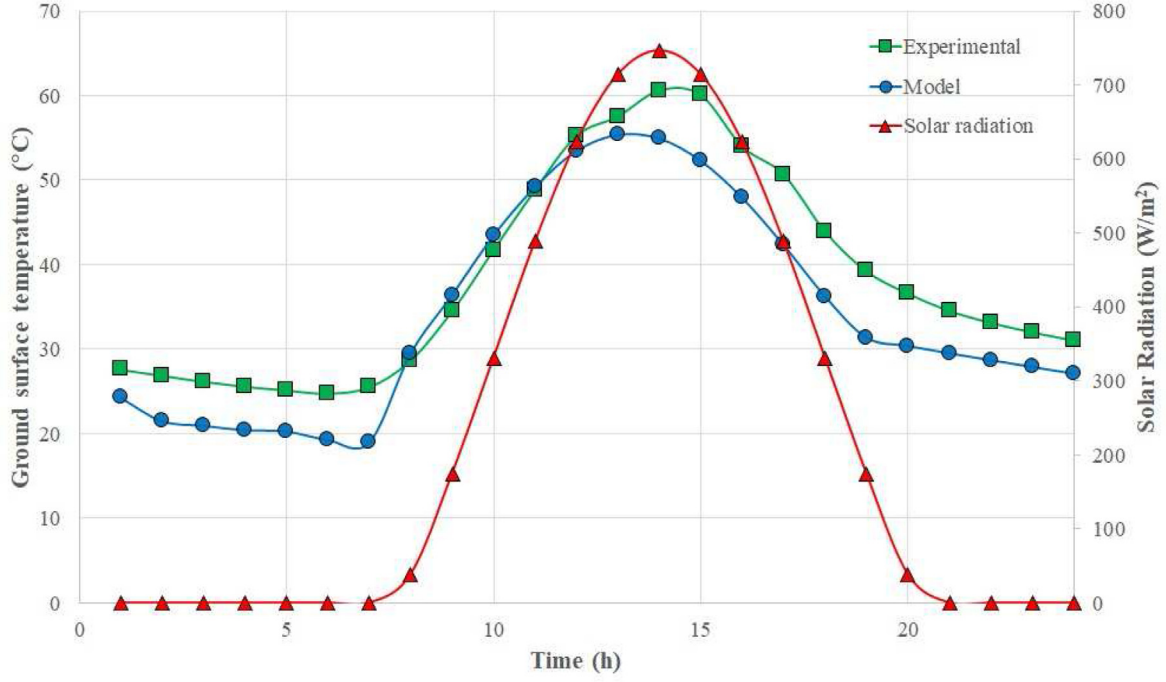

Fig. 7. Validation of the ground surface temperature.

incident solar radiation shown in Fig. 13 because it represents an average value.

Fig. 14 presents the monthly average ambient, outlet airflow, and ground surface temperatures. The inlet airflow temperature equals ambient temperature. As expected, the ground surface temperature is higher than the outlet airflow temperature, which is higher than the ambient temperature. On average, the ground surface temperature surpluses the outlet airflow temperature in 3.4 °C, which surpluses ambient temperature in 3.5 °C. The obtained values are lower than the maximum values in one day because they represent an average of the values. As can be seen in Figs. 6–8, for a specific day in October, the minimum and maximum ambient temperatures were 18.0 and 31.1 °C, the minimum and maximum outlet airflow temperatures were 18.8 and 45.8 °C, and

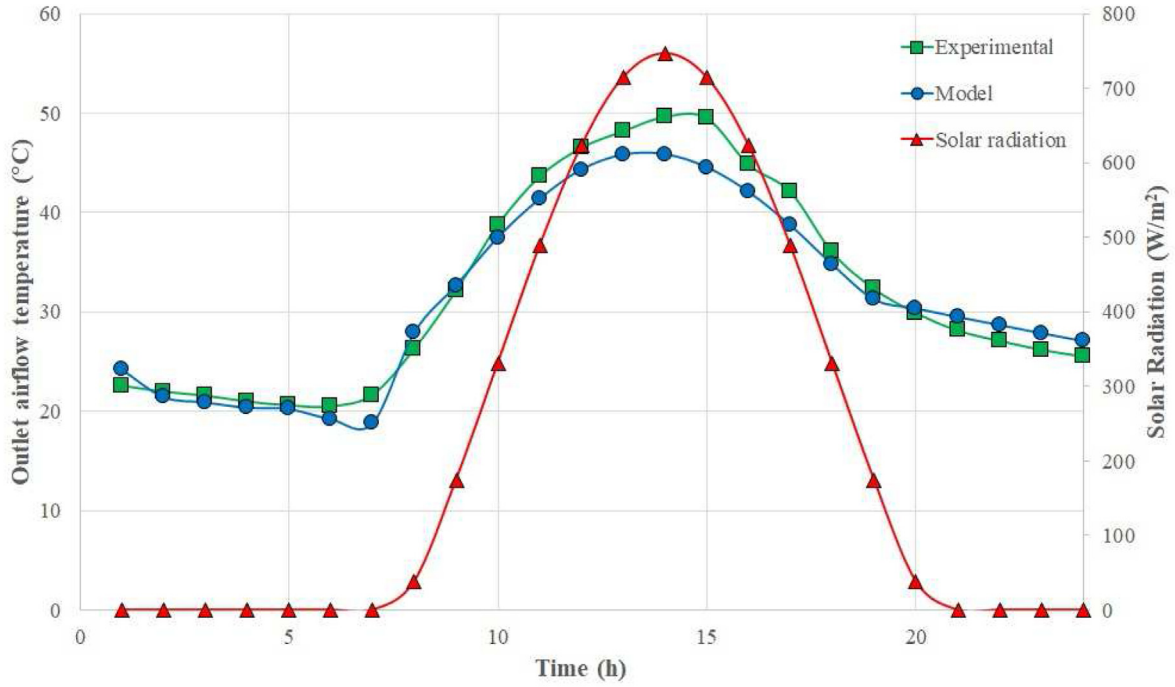

Fig. 8. Validation of the outlet airflow temperature.

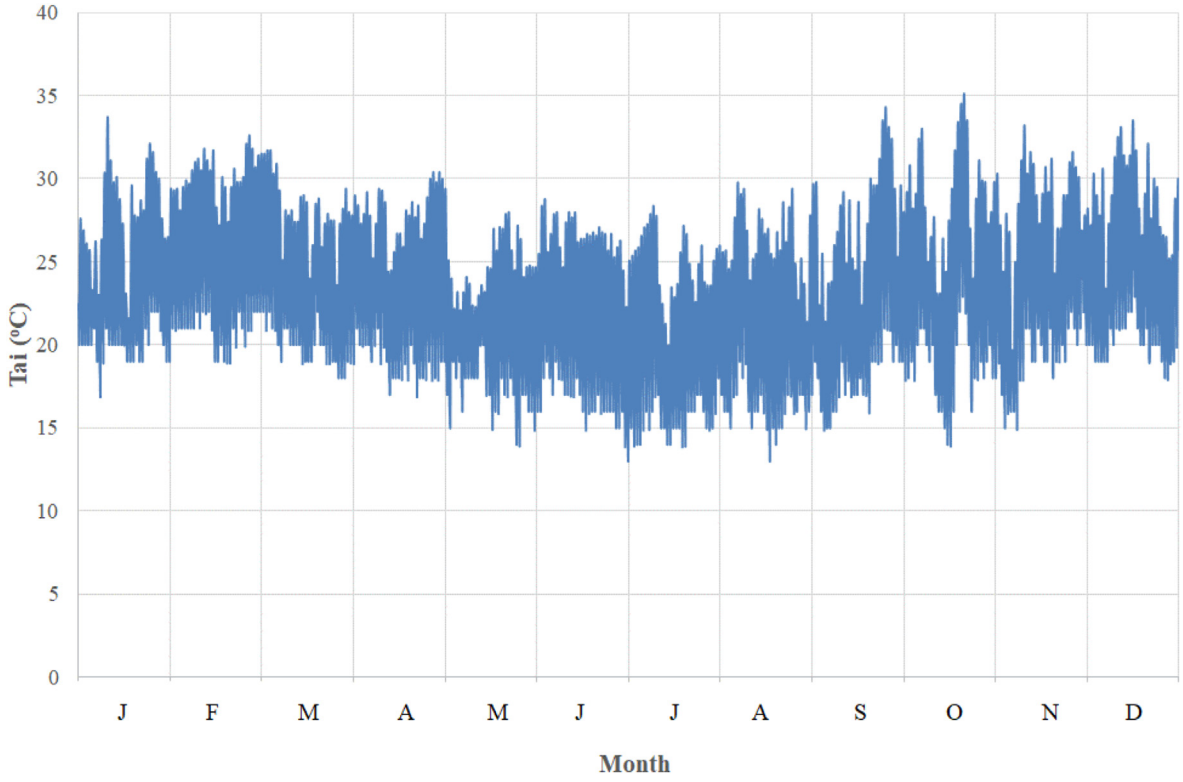

Fig. 9. Ambient temperature.

the minimum and maximum ground surface temperatures were 18.9 and 55.4 °C, resulting in average temperatures of 26.2, 31.5, and 34.4 °C, respectively, which are consistent with data from Fig. 14. For the same day, on average, the ground surface temperature surpluses the outlet airflow temperature in 7.1 °C, with a maximum of 15.6 °C, and the outlet airflow temperature surpluses ambient temperature in an average of 5.2 °C, with a maximum of 16.4 °C. The values are not equal, because data from Figs. 6–8 were obtained for a single day, and data from Fig. 14 represent the monthly average. Also, it is important to highlight that the behavior

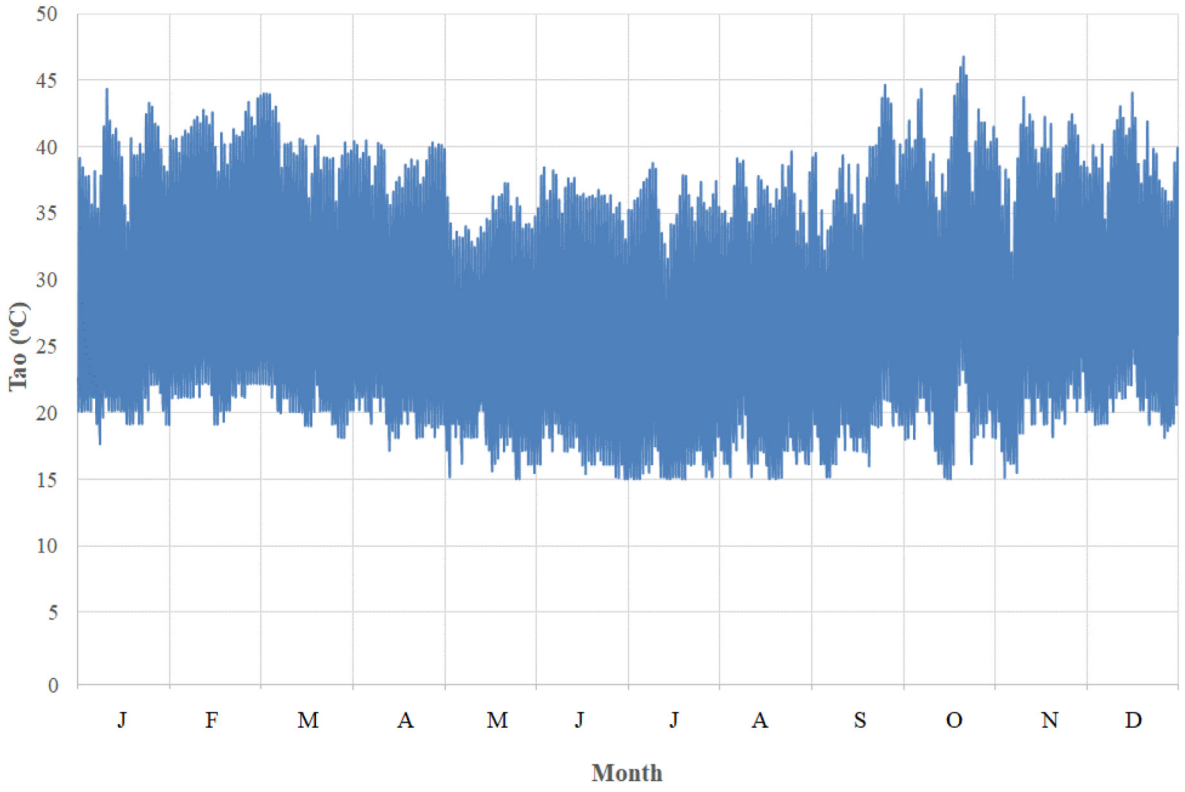

Fig. 10. Outlet airflow temperature.

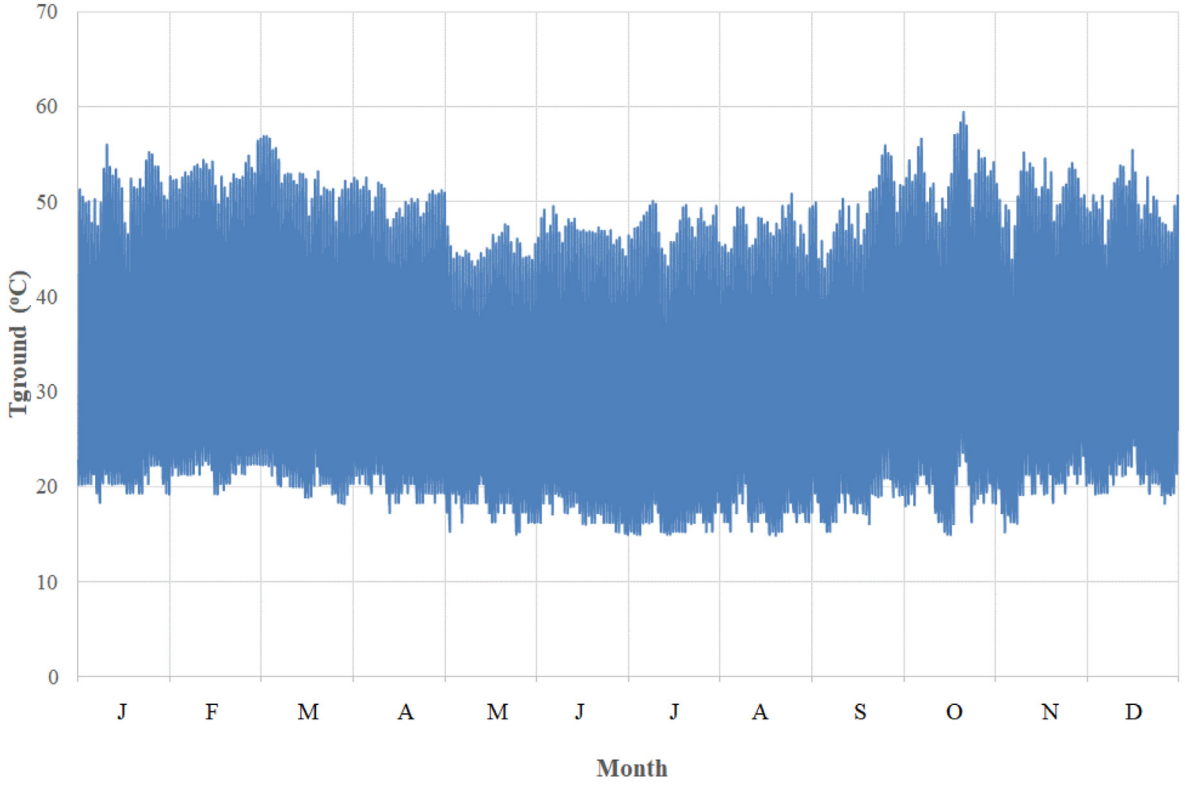

Fig. 11. Ground surface temperature.

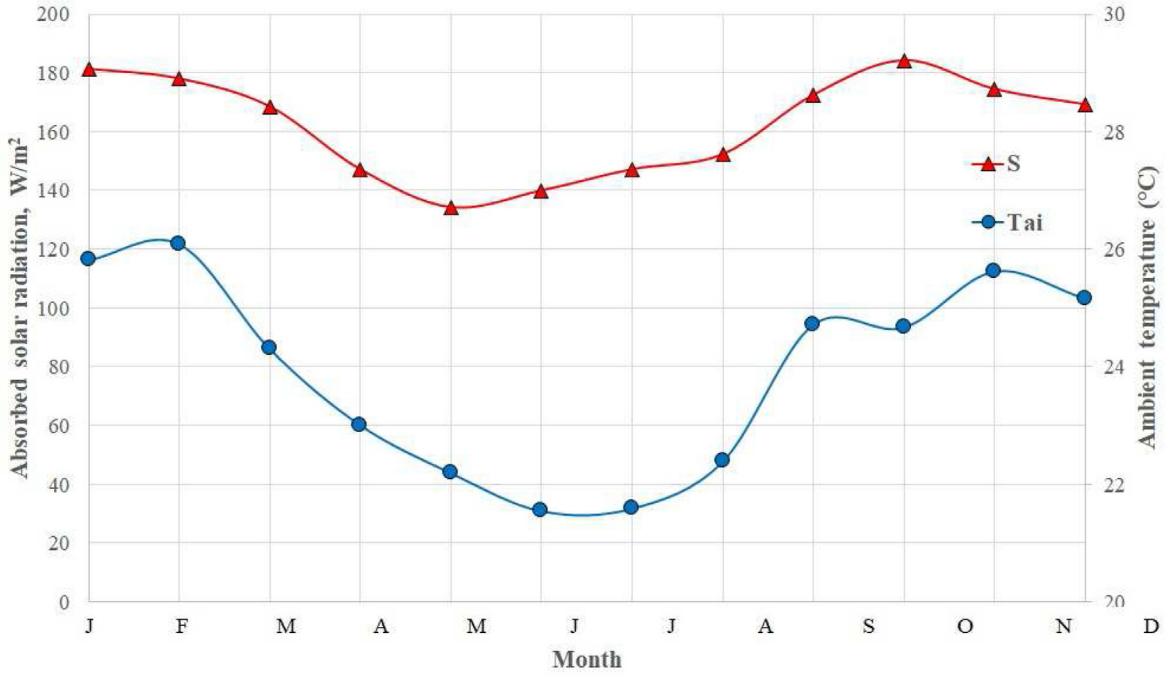

Fig. 12. Monthly averaged absorbed solar radiation and ambient temperature.

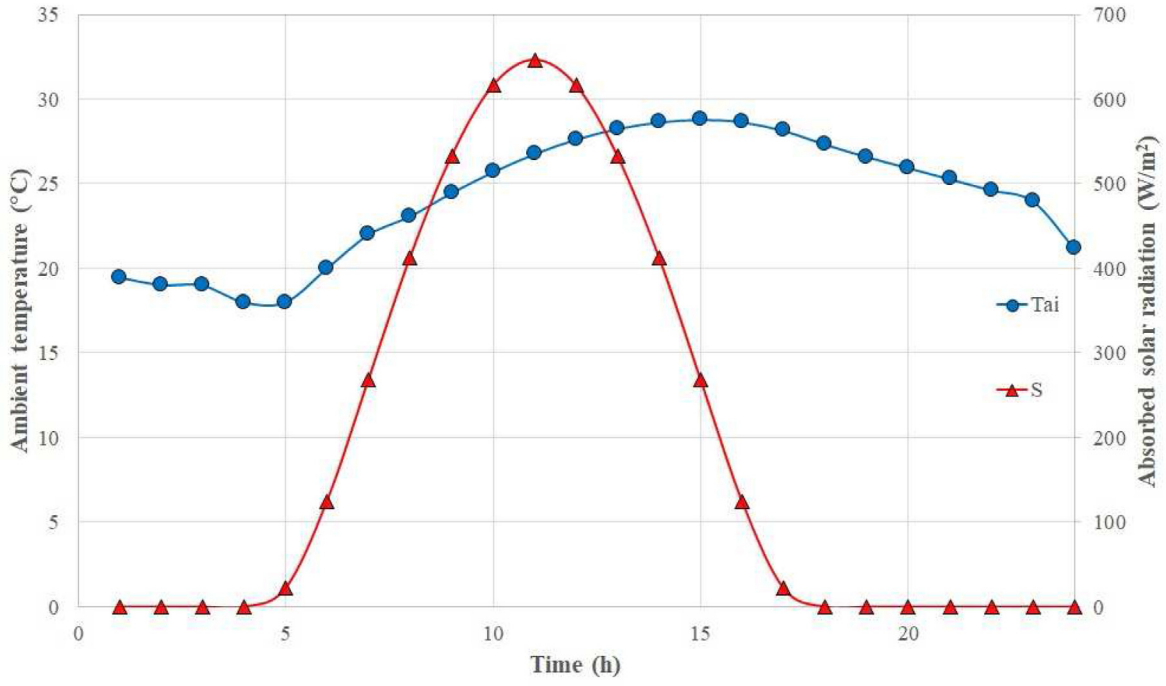

Fig. 13. Daily absorbed solar radiation and ambient temperature.

of the temperatures is similar to the absorbed solar radiation, as seen in Fig. 12.

The mass flowrate is an important parameter of the airflow because it represents the potential power production or drying rate. The airflow is generated by buoyancy forces, which means that the mass flowrate and the airflow velocity depend on the incident solar radiation and the ground surface temperature. For a fixed geometry, the higher the mass flowrate, the higher the velocity. The airflow velocity is highly dependent on the tower height, increasing with the tower height.

The heat transferred to the airflow also depends on the incident solar radiation and the ground surface temperature. The higher the incident solar radiation, the higher the ground surface temperature and the higher the heat absorbed by the airflow. Fig. 15 shows the daily numerical results for the mass flowrate and heat transfer rate for the same day of Figs. 6–8. It can be seen that the solar chimney

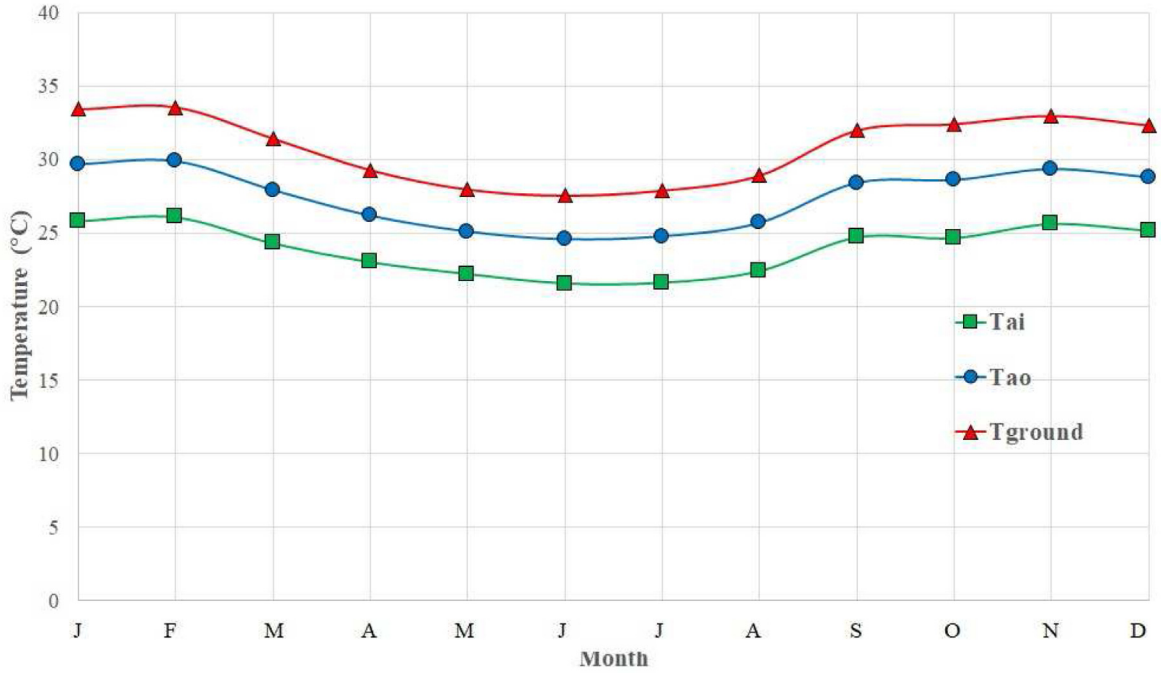

Fig. 14. Monthly averaged ambient and airflow temperatures.

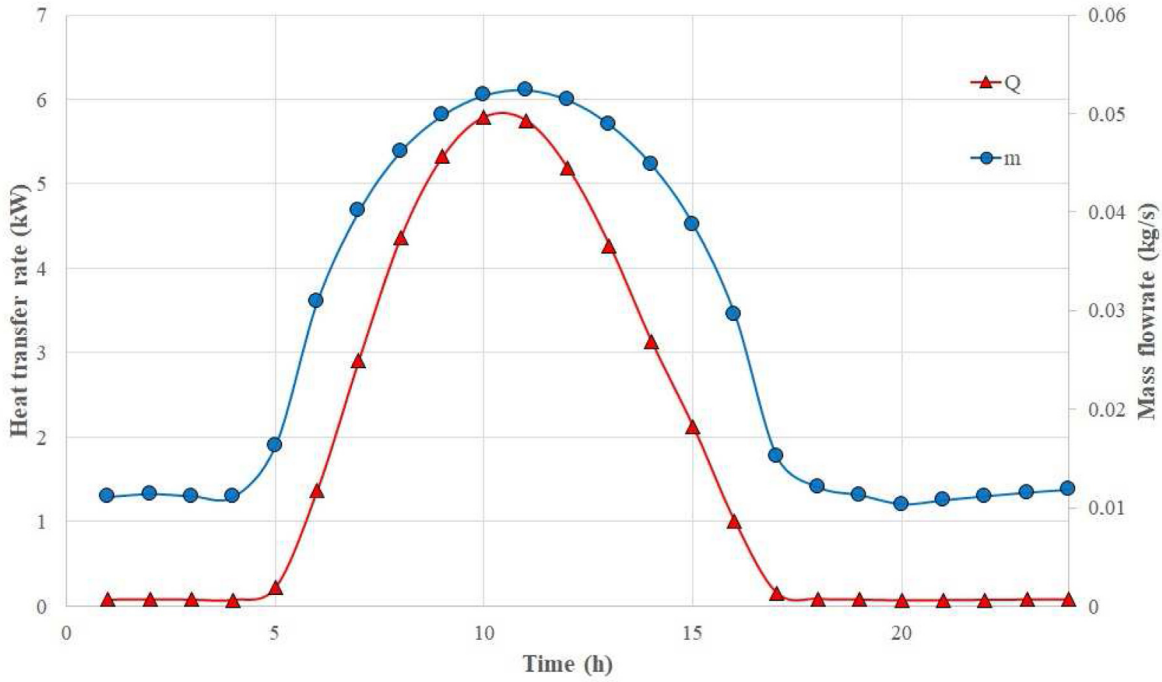

Fig. 15. Daily heat transfer rate and mass flowrate.

can generate a hot airflow even when there is no incidence of solar radiation because part of the heat absorbed by the deeper layers of the ground is released to the airflow during the night, ensuring a continuous functioning of the system.

Although the velocity and the mass flowrate vary during the day, the monthly average values did not suffer significant variations through the year, as can be seen in Fig. 16, with a maximum variation near 10%. The yearly average mass flowrate corresponds to a velocity of 0.76 m/s and a Reynolds of 1.1×10^5, characteristic of turbulent flow. Fig. 16 also shows the heat transfer rate received by the airflow. The minimum values were obtained in May, when the absorbed solar radiation is minimum, and the ambient temperature is low, resulting in high thermal losses to the environment.

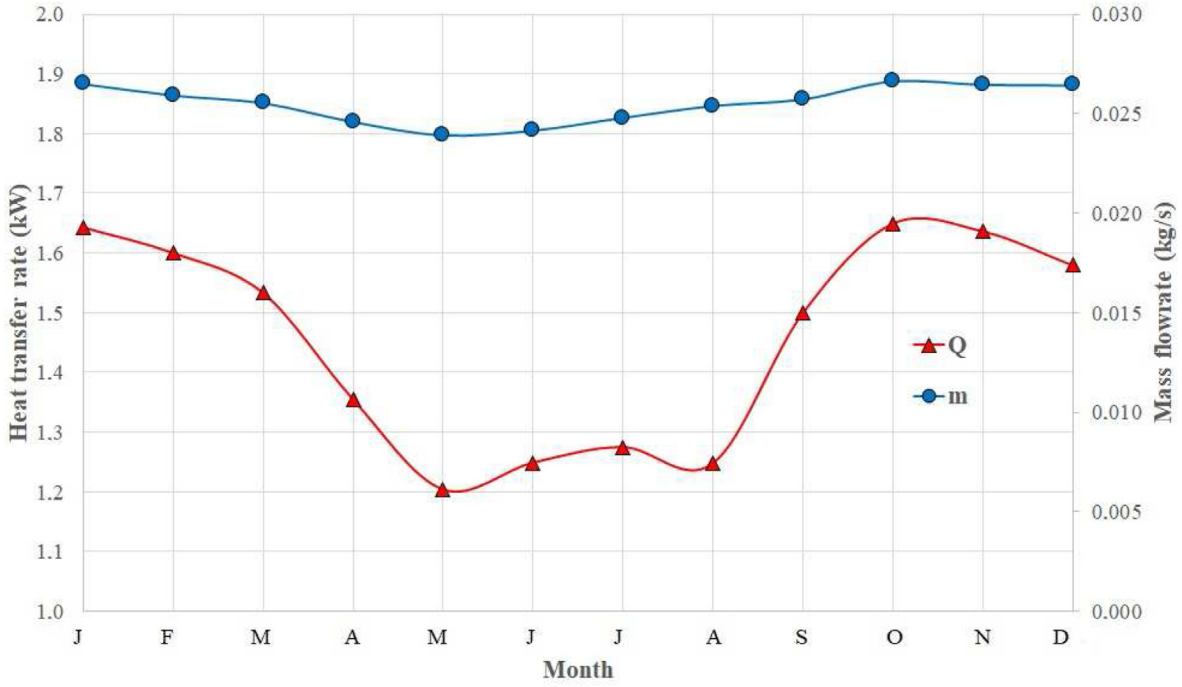

Fig. 16. Monthly averaged heat transfer rate and mass flowrate.

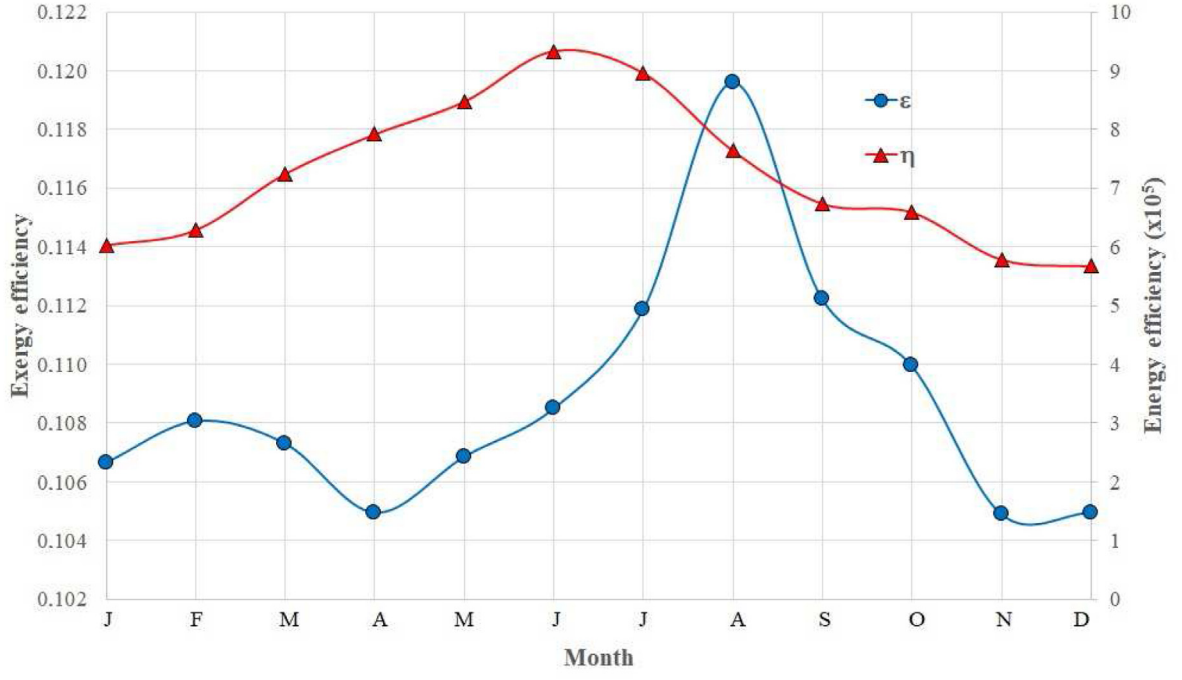

Fig. 17. Energy and exergy efficiency.

4.3. Thermodynamic analysis

The energy and exergy analysis of the system requires the knowledge of incident solar radiation, ambient, ground surface, and outlet airflow temperatures. These values were obtained from the mathematical model. Fig. 17 presents the monthly average energy and exergy efficiency of the system. The energy efficiency was very low, below 0.01%. This low value can be attributed to the small dimensions of the prototype. The maximum expected energy efficiency is 1% for devices up to 300 m [61], and the height of the prototype is only 2.5 m. It was found an average exergy efficiency of 11%. This prototype was built in a 1:5 scale to the prototype of [23,24]. For this system, the average exergy efficiency was about 20% when operated without load [24], and 27% when operated drying bananas [23]. It is known that the exergy efficiency increases with the chimney height [20], which can explain the lower values

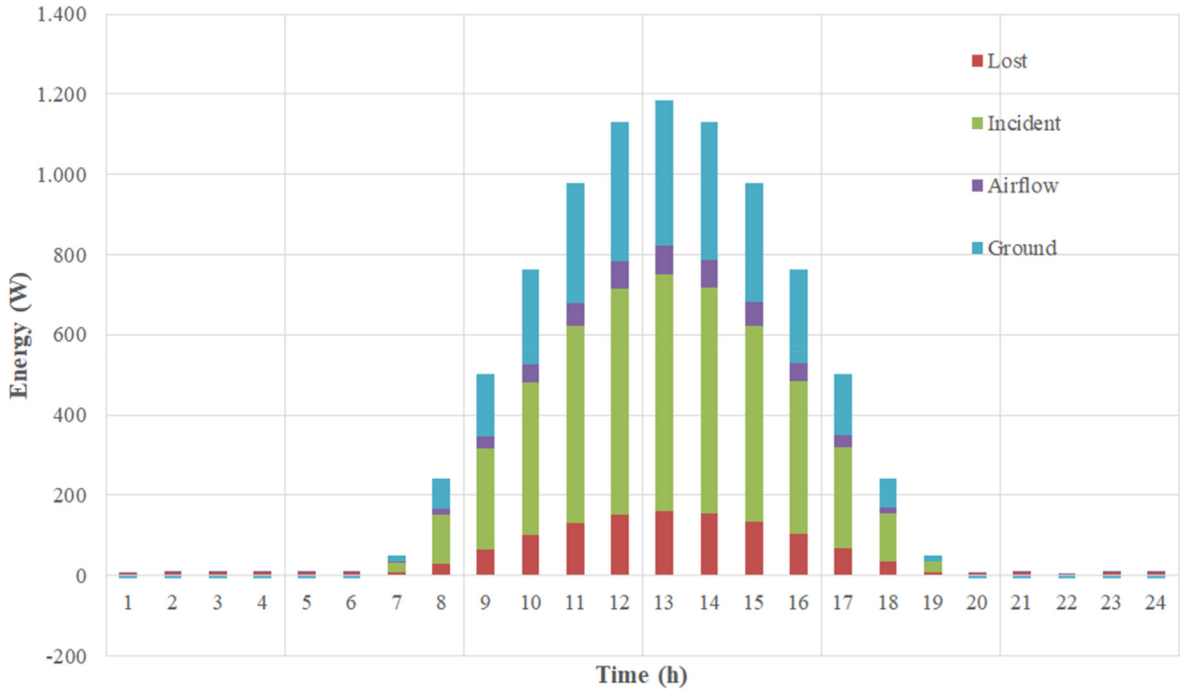

Fig. 18. Energy rates.

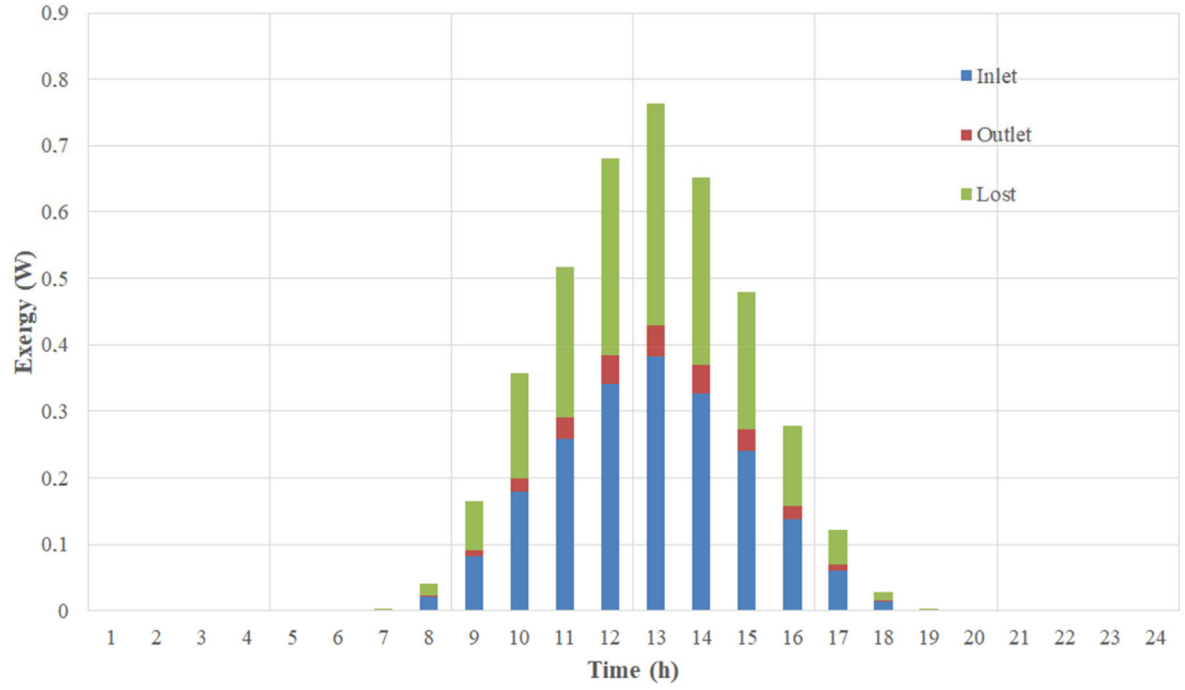

Fig. 19. Exergy rates.

found for the present paper. Also, when the system is operating with no load and no turbines, the hot airflow generated is lost, increasing the exergy losses and reducing the exergy efficiency.

To establish a correlation between the efficiency and the energy and exergy losses, Figs. 18 and 19 present the energy and exergy distribution. Fig. 18 shows that the incident energy (100%) is used to heat the ground (about 60%), heat losses (28%), and only 12% is used to heat the airflow, which justifies the lower energy efficiency. Fig. 19 shows that only about 13% of the exergy inlet is used by the airflow. Since the airflow is not used to run a turbine or to dry any products, most of the exergy is lost, and the exergy efficiency is also low. These results show that there is a great improvement potential in the system.

5. Conclusions

In this study, a mathematical model of a small-scale solar chimney is presented. The results were obtained for a full year of simulation, on an hourly basis. It was possible to evaluate the daily behavior of weather and airflow parameters, as well as monthly averaged values of the same parameters.

Numerical predictions from the mathematical model were compared to experimental results from a prototype designed and built in Belo Horizonte, Brazil. The performance of the solar chimney was assessed based on a thermodynamic analysis. In general, it was concluded that the results of the mathematical model can represent the parameters of the airflow, with the differences attributed also to expected variations of the weather parameters. The airflow parameters are strongly dependent on the weather conditions. The absorbed solar radiation and the ground surface temperature increase with the incident solar radiation. Since the airflow is heated by the ground and generated by the buoyancy forces, the outlet airflow temperature and the mass flowrate increase with the solar radiation. The energy and exergy efficiencies were low, but consistent with the dimensions of the prototype. The energy efficiency is highly dependent on the tower height, and the maximum expected value is 1%, for a solar chimney 300 m high. The exergy efficiency increases with the tower height, but the low value can be also attributed to the fact that the hot airflow generated was not used to drive a turbine or to dry agricultural products, increasing the exergy losses.

CRediT authorship contribution statement

Cristiana Brasil Maia: Conceptualization, Investigation, Writing – original draft, Writing – review & editing. **Janaína de Oliveira Castro Silva:** Resources, Investigation.

Declaration of competing interest

The authors declare that they have no known competing financial interests or personal relationships that could have appeared to influence the work reported in this paper.

Acknowledgments

This study was financing in part by the Coordenação de Aperfeiçoamento de Pessoal de Nível Superior - Brasil (CAPES) - Finance Code 001. The authors are also thankful to PUC Minas, FAPEMIG, and CNPq.

References

[1] Ren21, Facts from the renewables 2021 global status report -Trends in Brazil, Renewables 2021 Global Status Report 1 (2021) 1–2. https://www.ren21.net/wp-content/uploads/2019/05/REN21_GSR2021_Factsheet_Brazil_EN.pdf, 2021.
[2] L.E. Nunes, M.V.A. de Lima, M. Davison, A.L. da S. Leite, Switch and defer option in renewable energy projects: evidences from Brazil, Energy 231 (2021), https://doi.org/10.1016/j.energy.2021.120972.
[3] A. Boretti, S. Al-Zubaidy, Maturity assessment of the solar updraft tower technology, Renew. Energy Focus 27 (2018) 135–144, https://doi.org/10.1016/j.ref.2018.10.001.
[4] K. Chen, J. Wang, Y. Dai, Y. Liu, Thermodynamic analysis of a lowerature waste heat recovery system based on the concept of solar chimney, Energy Convers. Manag. 80 (2014) 78–86, https://doi.org/10.1016/j.enconman.2014.01.007.
[5] J. Schlaich, The Solar Chimney: Electricity from the Sun, 2002. Stuttgart.
[6] W. Haaf, Solar chimneys - Part II: preliminary test results from the Manzanares pilot plant, Int. J. Sol. Energy 2 (1984) 141–161, https://doi.org/10.1080/01425918408909921.
[7] E.Ö. Yapıcı, E. Ayli, O. Nsaif, Numerical investigation on the performance of a small scale solar chimney power plant for different geometrical parameters, J. Clean. Prod. (2020), https://doi.org/10.1016/j.jclepro.2020.122908.
[8] C.B. Maia, A.G. Ferreira, R.M. Valle, M.F.B. Cortez, Theoretical evaluation of the influence of geometric parameters and materials on the behavior of the airflow in a solar chimney, Comput. Fluids 38 (2009a) 625–636, https://doi.org/10.1016/j.compfluid.2008.06.005.
[9] A.G. Ferreira, C.B. Maia, M.F.B. Cortez, R.M. Valle, Technical feasibility assessment of a solar chimney for food drying, Sol. Energy 82 (2008) 198–205, https://doi.org/10.1016/j.solener.2007.08.002.
[10] M.A. Leon, S. Kumar, S.C. Bhattacharya, A comprehensive procedure for performance evaluation of solar food dryers, Renew. Sustain. Energy Rev. (2002), https://doi.org/10.1016/S1364-0321(02)00005-9.
[11] a.B. Kasaeian, E. Heidari, S.N. Vatan, Experimental investigation of climatic effects on the efficiency of a solar chimney pilot power plant, Renew. Sustain. Energy Rev. 15 (2011) 5202–5206, https://doi.org/10.1016/j.rser.2011.04.019.
[12] Mehran Ghalamchi, A. Kasaeian, Mehrdad Ghalamchi, Experimental study of geometrical and climate effects on the performance of a small solar chimney, Renew. Sustain. Energy Rev. (2015), https://doi.org/10.1016/j.rser.2014.11.068.
[13] Mehrdad Ghalamchi, A. Kasaeian, Mehran Ghalamchi, A.H. Mirzahosseini, An experimental study on the thermal performance of a solar chimney with different dimensional parameters, Renew. Energy 91 (2016) 477–483, https://doi.org/10.1016/j.renene.2016.01.091.
[14] N. Fadaei, A. Kasaeian, A. Akbarzadeh, S.H. Hashemabadi, Experimental investigation of solar chimney with phase change material (PCM), Renew. Energy 123 (2018) 26–35, https://doi.org/10.1016/j.renene.2018.01.122.
[15] H.H. Al-Kayeim, M.A. Aurybi, S.I.U. Gilani, Influence of canopy condensate film on the performance of solar chimney power plant, Renew. Energy 136 (2019), https://doi.org/10.1016/j.renene.2019.01.067.
[16] R. Balijepalli, V.P. Chandramohan, K. Kirankumar, Performance parameter evaluation, materials selection, solar radiation with energy losses, energy storage and turbine design procedure for a pilot scale solar updraft tower, Energy Convers. Manag. 150 (2017) 451–462, https://doi.org/10.1016/j.enconman.2017.08.043.
[17] P. Das, V.P. Chandramohan, Computational study on the effect of collector cover inclination angle, absorber plate diameter and chimney height on flow and performance parameters of solar updraft tower (SUT) plant, Energy 172 (2019) 366–379, https://doi.org/10.1016/j.energy.2019.01.128.
[18] P. Das, V.P. Chandramohan, 3D numerical study on estimating flow and performance parameters of solar updraft tower (SUT) plant: impact of divergent angle of chimney, ambient temperature, solar flux and turbine efficiency, J. Clean. Prod. 256 (2020), https://doi.org/10.1016/j.jclepro.2020.120353.
[19] P. Das, V.P. Chandramohan, Experimental studies of a laboratory scale inclined collector solar updraft tower plant with thermal energy storage system, J. Build. Eng. 41 (2021) 102394, https://doi.org/10.1016/j.jobe.2021.102394.
[20] M.O. Hamdan, Analysis of solar chimney power plant utilizing chimney discrete model, Renew. Energy 56 (2013) 50–54, https://doi.org/10.1016/j.renene.2012.09.047.
[21] C. Méndez, Y. Bicer, Integration of solar chimney with desalination for sustainable water production: a thermodynamic assessment, Case Stud. Therm. Eng. 21 (2020), https://doi.org/10.1016/j.csite.2020.100687.
[22] M. Aligholami, Sh Khosroshahi, A. SR Khosroshahi, Hydrodynamic and thermodynamic enhancement of a solar chimney power plant, Sol. Energy 191 (2019) 180–192, https://doi.org/10.1016/j.solener.2019.08.060.
[23] C.B. Maia, A.G. Ferreira, L. Cabezas-Gómez, J. de O. Castro Silva, S. de M. Hanriot, Thermodynamic analysis of the drying process of bananas in a small- scale solar updraft tower in Brazil, Renew. Energy 114 (2017) 1005–1012, https://doi.org/10.1016/j.renene.2017.07.102.
[24] C.B. Maia, J.O. Castro Silva, L. Cabezas-Gómez, S.M. Hanriot, A.G. Ferreira, Energy and exergy analysis of the airflow inside a solar chimney, Renew. Sustain. Energy Rev. 27 (2013) 350–361, https://doi.org/10.1016/j.rser.2013.06.020.
[25] A. Koonsrisuk, Mathematical modeling of sloped solar chimney power plants, Energy 47 (2012), https://doi.org/10.1016/j.energy.2012.09.039.
[26] A. Ayadi, A. Bouabidi, Z. Driss, M.S. Abid, Experimental and numerical analysis of the collector roof height effect on the solar chimney performance, Renew. Energy 115 (2018) 649–662, https://doi.org/10.1016/j.renene.2017.08.099.
[27] A. Ayadi, Z. Driss, A. Bouabidi, M.S. Abid, Experimental and numerical study of the impact of the collector roof inclination on the performance of a solar chimney power plant, Energy Build. 139 (2017) 263–276, https://doi.org/10.1016/j.enbuild.2017.01.047.
[28] M.A.H. Abdelmohimen, S.A. Algarni, Numerical investigation of solar chimney power plants performance for Saudi Arabia weather conditions, Sustain. Cities Soc. 38 (2018) 1–8, https://doi.org/10.1016/j.scs.2017.12.013.
[29] R. Rabehi, A. Chaker, T. Ming, T. Gong, Numerical simulation of solar chimney power plant adopting the fan model, Renew. Energy 126 (2018) 1093–1101, https://doi.org/10.1016/j.renene.2018.04.016.
[30] M.R. Torabi, M. Hosseini, O.A. Akbari, H.H. Afrouzi, D. Toghraie, A. Kashani, A. Alizadeh, Investigation the performance of solar chimney power plant for improving the efficiency and increasing the outlet power of turbines using computational fluid dynamics, Energy Rep. 7 (2021), https://doi.org/10.1016/j.egyr.2021.07.044.
[31] R.B. Weli, S.A. Atrooshi, R. Schwarze, Investigation of the performance parameters of a sloped collector solar chimney model – an adaptation for the North of Iraq, Renew. Energy 176 (2021) 504–519, https://doi.org/10.1016/j.renene.2021.05.075.
[32] F. Attig-Bahar, M.S. Guellouz, M. Sahraoui, S. Kaddeche, Economic analysis of a 1 MW solar chimney power plant in Tozeur, Tunisia, Renew. Energy 178

(2021), https://doi.org/10.1016/j.renene.2021.06.073.
[33] S.H. Fallah, M.S. Valipour, Numerical investigation of a small scale sloped solar chimney power plant, Renew. Energy 183 (2022) 1–11, https://doi.org/10.1016/j.renene.2021.10.081.
[34] D. Krumar Mandal, S. Pradhan, R. Chakraborty, A. Barman, N. Biswas, Experimental investigation of a solar chimney power plant and its numerical verification of thermo-physical flow parameters for performance enhancement, Sustain. Energy Technol. Assessments 50 (2022) 101786, https://doi.org/10.1016/j.seta.2021.101786.
[35] A. Koonsrisuk, T. Chitsomboon, Effects of flow area changes on the potential of solar chimney power plants, Energy 51 (2013) 400–406, https://doi.org/10.1016/j.energy.2012.12.051.
[36] M.A. Aurybi, S.I. Gilani, H.H. Al-Kayiem, A.A. Ismaeel, Mathematical evaluation of solar chimney power plant collector, integrated with external heat source for non-interrupted power generation, Sustain. Energy Technol. Assessments 30 (2018), https://doi.org/10.1016/j.seta.2018.06.012.
[37] P.J. Cottam, P. Duffour, P. Lindstrand, P. Fromme, Solar chimney power plants – dimension matching for optimum performance, Energy Convers. Manag. 194 (2019), https://doi.org/10.1016/j.enconman.2019.04.074.
[38] M. Setareh, Comprehensive mathematical study on solar chimney powerplant, Renew. Energy 175 (2021), https://doi.org/10.1016/j.renene.2021.05.017.
[39] P. Guo, Yunfeng Wang, J. Li, Yuan Wang, Thermodynamic analysis of a solar chimney power plant system with soil heat storage, Appl. Therm. Eng. 100 (2016) 1076–1084, https://doi.org/10.1016/j.applthermaleng.2016.03.008.
[40] F. Cao, Q. Liu, T. Yang, T. Zhu, J. Bai, L. Zhao, Full-year simulation of solar chimney power plants in Northwest China, Renew. Energy 119 (2018), https://doi.org/10.1016/j.renene.2017.12.022.
[41] F. Cao, H. Li, L. Zhao, T. Bao, L. Guo, Design and simulation of the solar chimney power plants with TRNSYS, Sol. Energy 98 (2013) 23–33, https://doi.org/10.1016/j.solener.2013.05.022.
[42] J.A. Duffie, W.A. Beckman, Solar Engineering of Thermal Processes, fourth ed., 2013, https://doi.org/10.1002/9781118671603.
[43] n.d. Swera, Solar and Wind Energy Resource Assessment (SWERA) [WWW Document]. URL, https://openei.org/apps/SWERA//. (Accessed 11 August 2018).
[44] Meteonorm, Meteonorm - Global Meteorological Database, 2012 [WWW Document]. Meteotest. URL, http://meteonorm.com/.
[45] Sinda, Hystorical data from sinda [WWW Document]. URL, http://sinda.crn.inpe.br/PCD/SITE/novo/site/historico/index.php, 2018.
[46] M.A.S. Bernardes, A. Voß, G. Weinrebe, Thermal and technical analyses of solar chimneys, Sol. Energy 75 (2003) 511–524, https://doi.org/10.1016/j.solener.2003.09.012.
[47] J. Yin Li, P. Hua Guo, Y. Wang, Effects of collector radius and chimney height on power output of a solar chimney power plant with turbines, Renew. Energy 47 (2012) 21–28, https://doi.org/10.1016/j.renene.2012.03.018.
[48] J.P. Pretorius, Optimization and Control of a Large-Scale Solar Chimney Power Plant, University of Stellenbosch, 2007.
[49] C.B. Maia, Análise Teórica e Experimental de uma Chaminé Solar: Avaliação Termofluidodinâmica, Universidade Federal de Minas Gerais, 2005.
[50] M.N. Ozisik, Heat Conduction, Book, 1993.
[51] D.G. Kröger, M. Burger, Experimental convection heat transfer coefficient on a horizontal surface exposed to the natural environment, in: Proceedings of the ISES EuroSun2004 International Sonnenforum, 2004, pp. 422–430.
[52] A. Koonsrisuk, S. Lorente, A. Bejan, Constructal solar chimney configuration, Int. J. Heat Mass Tran. 53 (2010) 327–333, https://doi.org/10.1016/j.ijheatmasstransfer.2009.09.026.
[53] J. de O. Castro Silva, Modelagem do escoamento de ar e otimização de uma chaminé solar, Pontifícia Universidade Católica de Minas Gerais, 2014.
[54] S. Nizetic, N. Ninic, B. Klarin, Analysis and feasibility of implementing solar chimney power plants in the Mediterranean region, Energy 33 (2008) 1680–1690, https://doi.org/10.1016/j.energy.2008.05.012.
[55] A.R. Celma, F. Cuadros, Energy and exergy analyses of OMW solar drying process, Renew. Energy 34 (2009) 660–666, https://doi.org/10.1016/j.renene.2008.05.019.
[56] M.G. Alpuche, C. Heard, R. Best, J. Rojas, Exergy analysis of air cooling systems in buildings in hot humid climates, Appl. Therm. Eng. 25 (2005) 507–517, https://doi.org/10.1016/j.applthermaleng.2004.07.006.
[57] M.C. Peel, B.L. Finlayson, T.A. McMahon, Updated world map of the Köppen-Geiger climate classification, Hydrol. Earth Syst. Sci. 11 (2007) 1633–1644, https://doi.org/10.5194/hess-11-1633-2007.
[58] M.S. Reboita, M. Rodrigues, L.F. Silva, M.A. Alves, Aspectos climáticos do estado de Minas Gerais, Rev. Bras. Climatol. 18 (2016) 307–326, https://doi.org/10.5380/abclima.v17i0.41493.
[59] C.B. Maia, A.G. Ferreira, R.M. Valle, M.F.B. Cortez, Analysis of the airflow in a prototype of a solar chimney dryer, Heat Tran. Eng. 30 (2009b) 393–399, https://doi.org/10.1080/01457630802414797.
[60] R.J. Moffat, Describing the uncertainties in experimental results, Exp. Therm. Fluid Sci. 1 (1988) 3–17, https://doi.org/10.1016/0894-1777(88)90043-X.
[61] T. Ming, W. Liu, G. Xu, Analytical and numerical investigation of the solar chimney power plant systems, Int. J. Energy Res. (2006), https://doi.org/10.1002/er.1191.